Geochemical Perspectives Letters

Concentration of meteoritic free organic matter by fluid transport and adsorption

C. Potiszil, R. Tanaka, T. Ota, T. Kunihiro, K. Kobayashi, E. Nakamura

Supplementary Information

The Supplementary Information includes:

- Materials and Methodology
- Tables S-1 and S-2
- Figures S-1 to S-8
- Supplementary Information References

Materials and Methodology

An interior surface of the Murchison (CM2) meteorite and a serpentinite blank were exposed through chipping. The samples were observed carefully during the process, which enabled the identification of the fresh surfaces. All tools were either heated in an oven to 500 °C for 2 h and/or cleaned with distilled MeOH (we 1x further distilled HPLC grade MeOH, from Kanto Chemical Co.,Inc.), prior to chipping. The chipped Murchison sample (~2x2 mm in size) and the serpentinite blank were pressed (using a pre-baked stainless steel block in between the sample and mechanical press) into separate aluminium holders filled with indium, in order to obtain a level sample surface. The holders containing the indium were also cleaned prior to sample mounting. The cleaning process involved submersion firstly in water and then in MeOH and exposure to ultrasound for 20 mins in both cases. Subsequently, the holder and indium surface were washed with distilled MeOH 3 times.

Mapping of the FOM compounds present within Murchison was carried out immediately by DESI-OT-MS. A DESI apparatus (Prosolia Inc.) was attached to an Orbitrap Fusion Hybrid mass spectrometer (Thermo Scientific). The imaging was undertaken in a clean room at the Pheasant Memorial Laboratory, Institute for Planetary Materials, Okayama University. The clean room as a whole was found to be class 10, but the area surrounding the DESI-OT-MS was found to be class 1, due to the large HEPA unit located on the wall nearby. Note that the serpentinite blank was also imaged to check for contamination (Fig. S-3, S-4).

The DESI spray head was held at an angle of 62 ° with respect to the sample surface and the effective distance from the tip of the fused silica tube to the surface was ~3 mm. A gas pressure of ~0.75 MPa was used to spray distilled MeOH onto the sample surface at a rate of 3 μm/s during analysis. The scanning speed was set to 83.33 μm/s during analysis of the samples.

The resolution of the DESI is dependent on the diameter of the spray hitting the surface, the step size for the y-axis and the number of acquisitions per the sample length for the x-axis. The spray diameter is ~40 μm for the y-axis direction, as indicated by the thickness of a line created after passing 3 times across a spot of rhodamine dye. However, the DESI was stepped at 50 μm increments, so the actual y-axis resolution is 50 μm. The DESI was ran in continuous scanning mode and so a minimum x-axis resolution of 26.56 μm is possible, based on the number of acquisitions (128) per a row (3400 μm). Nevertheless, the actual x-axis resolution could be nearer to 40 μm, due to being limited by the spray diameter.

The parameters used for OT-MS are as follows: 50-500 m/z range, positive mode, 4000 V, 120,000 $m/\Delta m$ at m/z 200, an auto gain control of 2 x 10^5 and a maximum injection time of 50 ms. Mass calibration of the OT-MS was performed prior to installation of the DESI, using a heated-electrospray ionisation (H-ESI) source and Pierce™ LTQ ESI positive ion calibration solution (Thermo Scientific).

The DESI map was constructed from raw MS files, each file representing one row of the map, using the FireFly™ software (Prosolia Inc.). The map file was then viewed using MSiReader (version 1.0) (Bokhart *et al.*, 2018; Robichaud *et al.*, 2013) and individual masses relating to compounds from the literature were input to search for those demonstrating interesting 2D relationships. Note that the maps were normalised to the total ion current, which makes the sum of all ions for a given pixel equal across the map. As such the total ion current is the same for each pixel and thus the variation of intensity for a given mass can be assessed between pixels across the entire map.

DESI-OT-MS is potentially affected by surface topography, because variation in distance between the spray head, sample surface and inlet can influence the quantity of the extracted sample entering the instrument. Consequently, the sample was analysed with a laser profiler, using an Alicona InfiniteFocus SL at the Tottori Institute of Industrial Technology for the analysis of surface topography. The instrument has a vertical resolution of 50 nm and a lateral topographic resolution of 1 μm. With the exception of a small area associated with the central chondrule, the topography shows variation of ~80 μm (Fig. 1c). If the topographic variation was a major controller of the intensity of the DESI-OT-MS maps, then areas of high topography should correlate with areas of high intensity. Such a correlation is not observed for the DESI-OT-MS maps, especially for the higher molecular weight homologues.

Imaging of the sample surface was undertaken using a field-emission-type scanning electron microscope (FE-SEM), JSM-7001F (JEOL, Japan), under conditions of 15 kV acceleration voltage, 3 nA beam current, and without coating on the surface. A mosaic was generated from multiple images to give a detailed representation of the sample surface. The extracted single mass maps were then overlain onto an SEM image using Echo, a custom developed software and database at the Pheasant Memorial Laboratory. Rhodamine dye spots placed onto the surface of the indium close to the sample aided the matching of the DESI-OT-MS maps to the SEM image.

A Thermo Nicolet DXR confocal microscope was used to map the sample, with a Raman shift range of 50-6000 cm^{-1}. The corresponding spectral resolution was ~11 cm^{-1}. The spectral resolution is primarily dependent on the FWHM of the Raman signal detected. However, this is itself dependent on other factors, including the wavelength of the laser, but to a large extent on the line density of the grating used (400 lines/mm for the current study). The spot size of the laser was ~1.3 μm^2 and the map was collected with 20 μm steps in both the x and y direction across the entire sample. A 0.3 mW laser power was used for the 532 nm laser, in order to prevent alteration of the organic matter. Two exposures of 15 s were collected for each spot and combined to improve signal to noise and limit the effects of fluorescence and Rayleigh scattering. Maps were automatically baseline corrected and normalised using the Omnic Altμs software (Theromo Scientific). A profile map, representing the area intensity of the whole water feature between 3000-3800 cm^{-1} was then created using the Atlus software. Subsequently, the maps were split and selected spectra (Fig. S-7) manually baseline corrected and their peaks fitted using Fityk (Wojdyr, 2010). Initial identification of the peaks was undertaken with reference to the literature (Wang *et al.*, 2015a, 2015b) and fitting was undertaken in Fityk using a Levenberg-Marquardt algorithm, which is a standard nonlinear least-squares routine.

Despite normalisation of Raman data, sample topography might influence areas of high interlayer/adsorbed water band intensity. In order to ascertain the contribution of sample topography to the Raman intensity, two Raman maps were recorded, one focused on high topography (majority of sample above ~40 μm) (Fig. S-8a) and the other on low topography (majority of sample below ~40 μm) (Fig. S-8b). For the high topography map, interlayer/adsorbed water band intensity does tend to correlate with higher topographic areas (Fig. S-8a), but there are also high intensity areas which relate to low topography or cut topographic contours. The low topographic map (Fig. S-8b) mainly recorded high intensity areas for the lower topographic areas, although a large area was recorded for the top right portion of the sample. The large high intensity area might relate to phases below the surface, due to the focus of the laser influencing its penetration depth. Consequently, areas of high and low topography were highlighted for correlation maps in Figures 2 and 3 to aid communication of the relationships to readers. Note the Raman instrument was unable to accurately focus on the sample surface when using the autofocus option and thus this was not a viable way to mitigate topographic effects.

After Raman spectroscopy, quantitative analyses of major elements in mineral phases were undertaken using a FE-SEM, JSM-7001F, equipped with an EDX, AZtec X-Max, X-act (Oxford Instruments, UK). The analyses were conducted using a 15 kV acceleration voltage, 3 nA beam current, and 50 s integration times. Calibration for quantitative analyses were conducted using natural silicate minerals and synthetic oxides and alloys (JEOL reference materials). The EDX analyses were undertaken for phases within the chondrules and selected areas of the matrix, which had been identified as having a high intensity of adsorbed/interlayer water from Raman spectroscopy. Note that phase maps were not possible due to the unpolished surface, which lead to a poor oxide yield for many areas of the sample. Consequently, data was provided for spots that gave a good oxide yield.

Correlation maps were constructed from 3 DESI maps for each homologue series, masses were selected to represent LMW, IMW and HMW and 2 Raman maps, one for high topography (focused on the top ~40 μm of the sample) and one for low topography (focused so that the majority of the sample below 40 μm was in focus). The resolution of the DESI and Raman maps was increased by dividing the existing pixels within these maps into further pixels with the same intensity. The resolution was increased to reduce edge effects that could occur later when warping the Raman maps. The Raman maps were then aligned with the DESI images using a custom built software that allowed the rotating and warping of the images, whilst preserving the hard edges of the pixels. The Raman maps consisted of a greater number of pixels due to the higher spatial resolution (20 μm^2) than DESI images (~26x50 μm). As such the centres of the blocks of pixels of the same intensity, which related to the original Raman pixels before the resolution was increased, were marked using a MATLAB script written using Emacs. The intensity values of the blocks were then plotted against those of the corresponding area on the DESI map, in order to mitigate edge effects that could occur due to the non-rectangular shape of these blocks after warping.

Correlation diagrams of DESI/Raman were generated and showed no clear trend due to the complexity of the maps. Therefore, the intensity scales of the DESI and Raman were divided into three: low, intermediate and high intensity. Each plot of DESI/Raman was thus divided into 9 domains and a colour was assigned to each (Figs. 2d. and 3d.). Points from the DESI/Raman plots were then given the colour of the domain they plotted in and were placed onto a new map. The points were placed in the same location from which the intensity values had been obtained for the Raman and DESI maps. The new correlation maps thus enabled the assessment of how correlated a given pixel was, in terms of low, intermediate or high DESI *vs.* low, intermediate or high Raman intensity. The scripts used to create the correlation maps were written using Emacs and run in MATLAB.

Further correlation maps were made to compare the LMW and IMW homologues and the LMW and HMW homologues for both homologue series, in order to assess the presence of a geochromatographic effect. The DESI/DESI correlation maps were made in a similar way to the DESI/Raman maps, except due to the alignment being the same for all DESI images no warping or rotating was necessary.

Supplementary Tables

Table S-1 EDX data for the Murchison meteorite chip represented as oxide %. Location names refer to the positions indicated in figure 1a. CC = central chondrule, TLC = top left chondrule, MTR = matrix top right and MBC = matrix bottom centre. Ol. = olivine, Serp. = serpentine, Cron. = cronstedtite, LCP = low calcium pyroxene and CS = calcium sulfate. Note that whilst all the Fe has been allocated to FeO, there is most likely Fe2O3 present as well.

Location	Phase	NaO	MgO	Al_2O_3	SiO_2	S	K_2O	CaO	TiO_2	Cr_2O_3	MnO	FeO	NiO	Total
CC 1	Ol.	0.00	56.94	0.17	41.41	0.00	0.01	0.11	0.02	0.26	0.15	0.90	0.01	100.00
CC 2	Ol.	0.00	57.34	0.11	41.02	0.15	0.04	0.12	0.02	0.20	0.14	0.79	0.07	100.00
TLC 1	Ol.	1.01	49.91	0.63	39.55	0.00	0.12	0.25	0.05	1.18	0.15	6.88	0.25	100.00
TLC 2	Ol.	0.47	52.59	0.30	41.01	0.00	0.07	0.29	0.18	0.69	0.27	4.10	0.03	100.00
TLC 3	Serp./Cron.	0.97	17.22	2.22	29.76	8.95	0.26	0.73	0.08	0.62	0.39	36.30	2.51	100.00
TLC 4	Serp./Cron.	1.10	21.08	2.89	33.57	8.41	0.22	0.83	0.16	0.49	0.19	29.16	1.89	100.00
TLC 5	LCP	0.06	37.73	0.71	56.95	0.00	0.02	0.66	0.16	0.64	0.08	2.98	0.01	100.00
TLC 6	LCP	0.09	36.11	0.87	54.69	0.00	0.07	0.80	0.13	0.80	0.08	6.11	0.26	100.00
MTR 1	Serp./Cron.	0.66	16.05	3.29	29.26	9.79	0.27	0.28	0.18	0.23	0.33	37.88	1.78	100.00
MTR 2	Serp./Cron.	0.27	21.19	2.48	33.89	3.61	0.11	0.18	0.02	0.39	0.21	36.80	0.85	100.00
MBC 1	Serp./Cron.	0.38	17.16	2.22	32.19	6.34	0.38	0.40	0.17	0.41	0.39	38.45	1.52	100.00
MBC 2	Serp./Cron.	0.57	14.89	2.06	29.55	6.61	0.35	0.39	0.07	0.59	0.35	41.72	2.86	100.00
MBC 3	CS	0.77	5.66	0.58	11.17	42.59	0.32	29.10	0.04	0.13	0.01	9.18	0.48	100.00

Table S-2 DESI-OT-MS data for the alkylimidazoles and alkylpyridine homologues reported here. C# = carbon number. Diff. = difference in parts per a million (ppm) between the measured and calculated masses for the homologues.

Alkylimidazole				Alkylpyridine		
C#	Measured	Calculated	Diff. (ppm)	Measured	Calculated	Diff. (ppm)
7	125.10732	125.10733	-0.04	-	-	-
8	139.12293	139.12298	-0.30	122.09637	122.09643	-0.43
9	153.13854	153.13863	-0.54	136.11205	136.11208	-0.16
10	167.15416	167.15428	-0.71	150.12765	150.12773	-0.53
11	181.16978	181.16993	-0.81	164.14328	164.14338	-0.58
12	195.18540	195.18558	-0.90	178.15891	178.15903	-0.65
13	209.20103	209.20123	-0.92	192.17452	192.17468	-0.79
14	223.21666	223.21688	-0.95	206.19016	206.19033	-0.81
15	237.23225	237.23253	-1.18	220.20580	220.20598	-0.81
16	251.24789	251.24818	-1.15	234.22132	234.22163	-1.31

Supplementary Figures

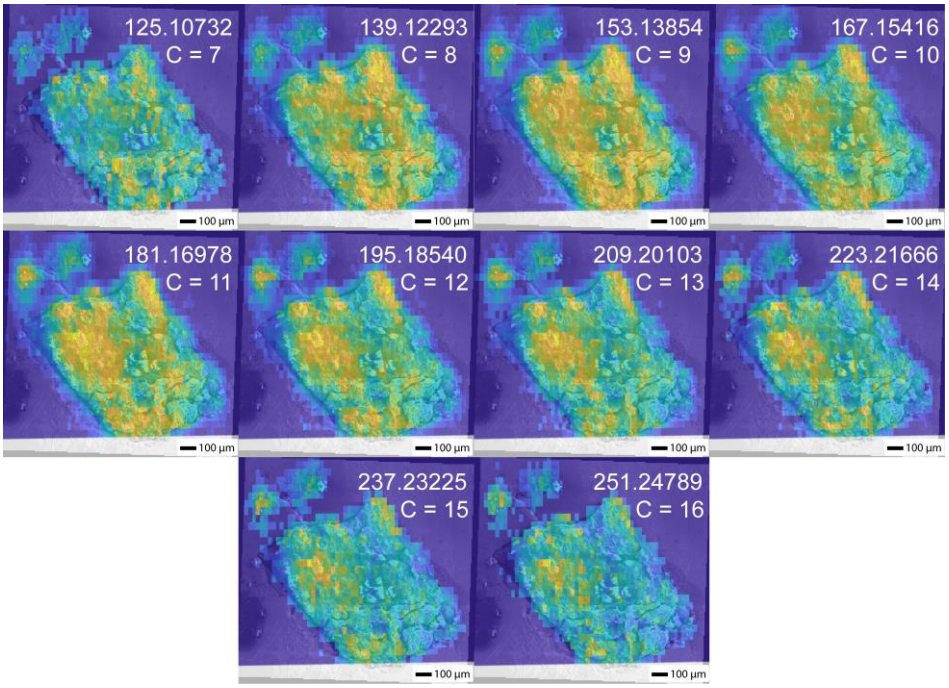

Figure S-1 Intensity maps of alkylimidazole homologues identified in Murchison. The maps were constructed from DESI-OT-MS data and placed onto SEM images. The scale for the DESI maps ranges from dark blue (not detected) to light blue, green, orange and then yellow (highest intensity). The masses of the detected ions and their corresponding carbon number are indicated on each image. The TIC normalised intensities for each map (in the order of occurrence on the figure) are: 3.04×10^{-3}, 8.79×10^{-3}, 1.27×10^{-2}, 1.47×10^{-2}, 1.22×10^{-2}, 9.89×10^{-3}, 7.37×10^{-3}, 5.37×10^{-3}, 3.84×10^{-3}, 2.70×10^{-3}.

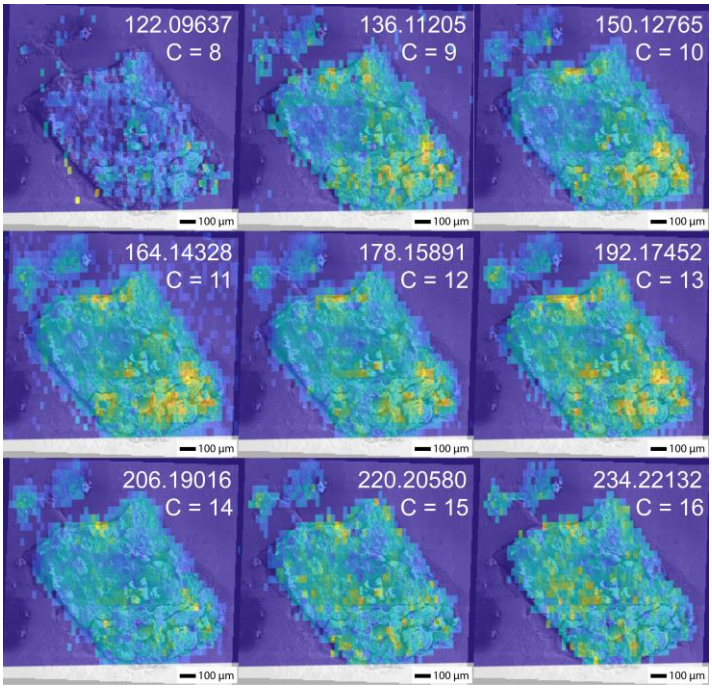

Figure S-2 Intensity maps of alkylpyridine homologues identified in Murchison. The maps were constructed from DESI-OT-MS data and placed onto SEM images. The scale for the DESI maps ranges from dark blue (not detected) to light blue, green, orange and then yellow (highest intensity). The masses of the detected ions and their corresponding carbon number are indicated on each image. The TIC normalised intensities for each map (in the order of occurrence on the figure) are: 1.33×10^{-3}, 2.17×10^{-3}, 3.74×10^{-3}, 5.03×10^{-3}, 5.44×10^{-3}, 4.00×10^{-3}, 3.76×10^{-3}, 2.58×10^{-3}, 1.92×10^{-3}.

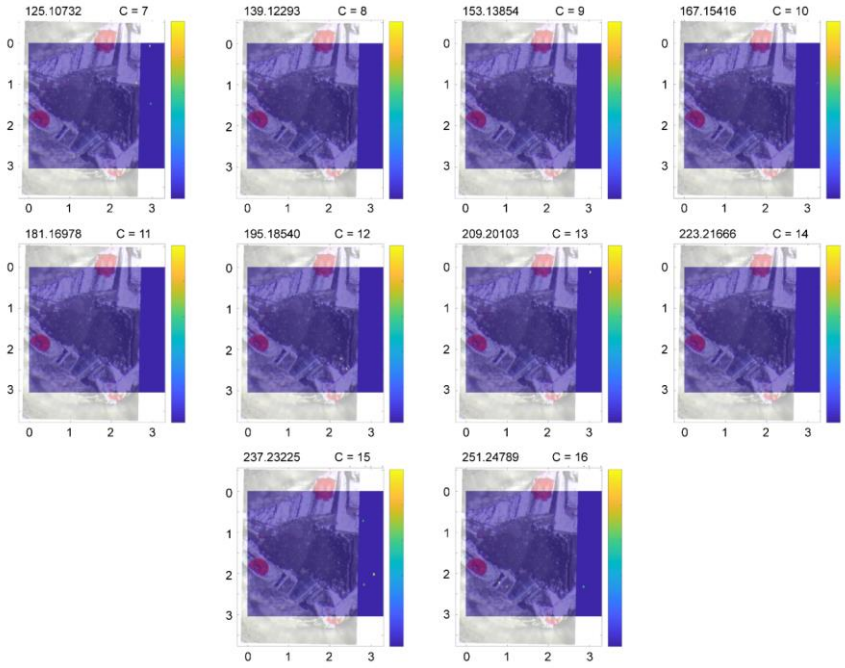

Figure S-3 DESI-OT-MS maps of the alkylimidazole homologue masses for a serpentinite blank, which have been overlain upon an optical microscope image. The blank was prepared in the same way as the Murchison sample. Axis are in mm and the intensity legend ranges from yellow (highest intensity) to dark blue (not detected). The TIC normalised intensities for each map (in the order of occurrence on the figure) are: 1.39×10^{-3}, below detection limit, 1.25×10^{-3}, 3.08×10^{-3}, below detection limit, 4.88×10^{-4}, 9.42×10^{-4}, 1.26×10^{-3}, 2.38×10^{-3}, 9.14×10^{-4}.

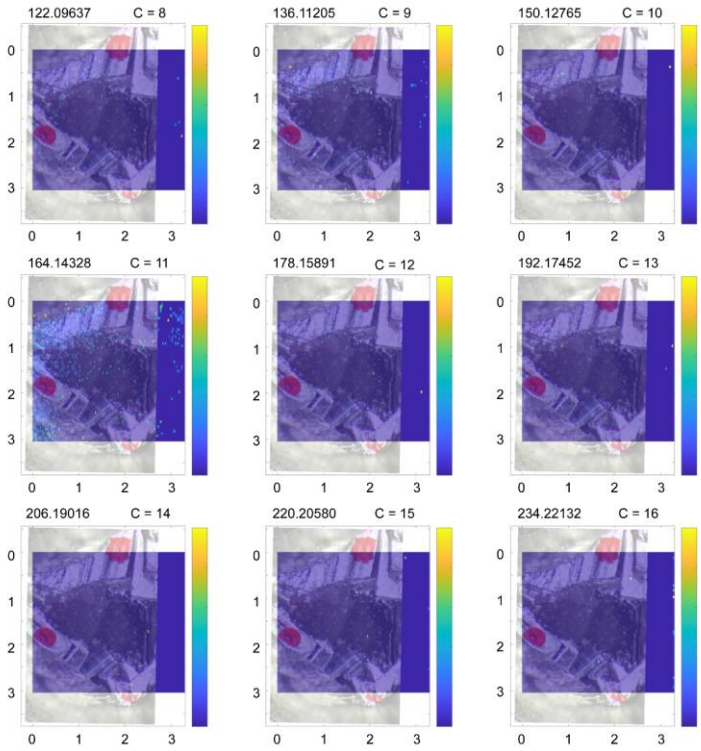

Figure S-4 DESI-OT-MS maps of the alkylpyridine homologue masses for a serpentinite blank, which have been overlain upon an optical microscope image. The blank was prepared in the same way as the Murchison sample. Axis are in mm and the intensity legend ranges from yellow (highest intensity) to dark blue (not detected). The TIC normalised intensities for each map (in the order of occurrence on the figure) are: 1.59×10^{-3}, 2.14×10^{-3}, 3.36×10^{-3}, 2.96×10^{-3}, 1.16×10^{-3}, 6.00×10^{-4}, 3.62×10^{-4}, 9.5×10^{-4}, 1.36×10^{-3}.

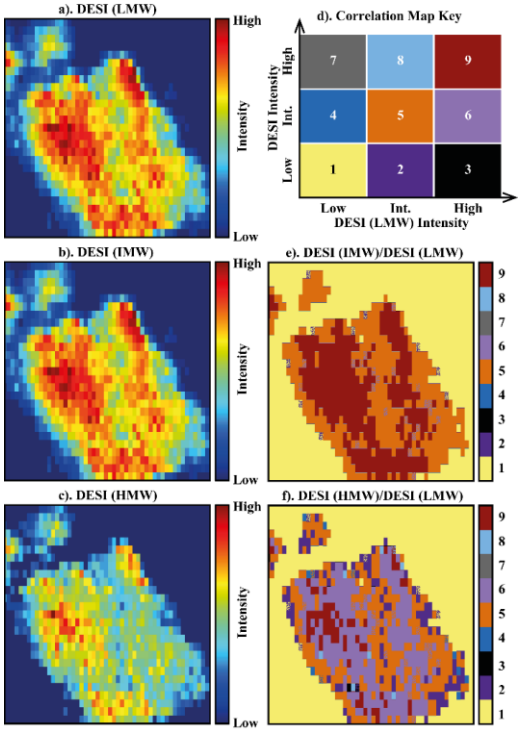

Figure S-5 A compilation of DESI and DESI/DESI correlation maps for selected alkylimidazole homologues. **(a-c)** DESI intensity maps for mass 139.12293, 181.16978 and 237.23225, respectively. **(d)** A schematic outlining the criteria for the generation of DESI *vs.* DESI correlation maps. **(e)** Correlation map showing the similarity/difference between the IMW and LMW DESI maps. **(f)** Correlation map showing the similarity/difference between the HMW and LMW DESI maps.

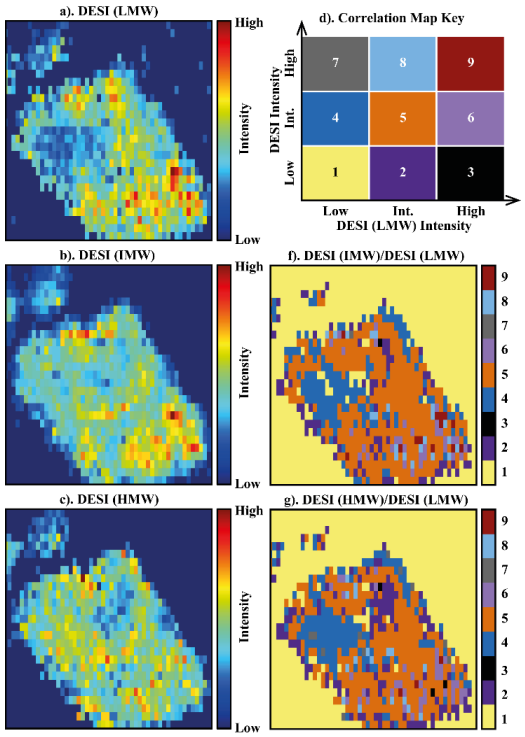

Figure S-6 A compilation of DESI and DESI/DESI correlation maps for selected alkylpyridine homologues. **(a-c)** DESI intensity maps for mass 136.11205, 178.15891 and 220.20580, respectively. **(d)** A schematic outlining the criteria for the generation of DESI *vs.* DESI correlation maps. **(e)** Correlation map showing the similarity/difference between the IMW and LMW DESI maps. **(f)** Correlation map showing the similarity/difference between the HMW and LMW DESI maps.

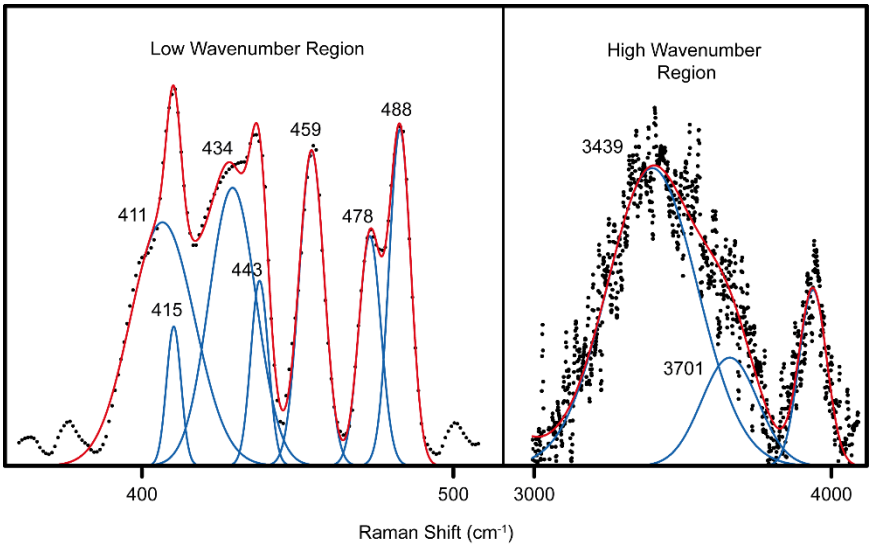

Figure S-7 Selected Raman spectra demonstrating features indicating the presence of phyllosilicates. Peaks of interest are labelled with their peak centres. Within the low wave number region, the peaks represent lattice modes. It is difficult to identify the specific phases, but they are consistent with a mixture of phyllosilicate compositions (Wang *et al.*, 2015a). The high wavenumber region records a broad feature within the H2O/OH region. The peak at 3439 cm^{-1} represents adsorbed/interlayer water, whilst the peak at 3701 cm^{-1} arises from the mineral OH group (Wang *et al.*, 2015a). Blue lines indicate fitted peaks, whilst red the resulting convolution. Note that the low wavenumber and high wave number regions were extracted from two different spectra.

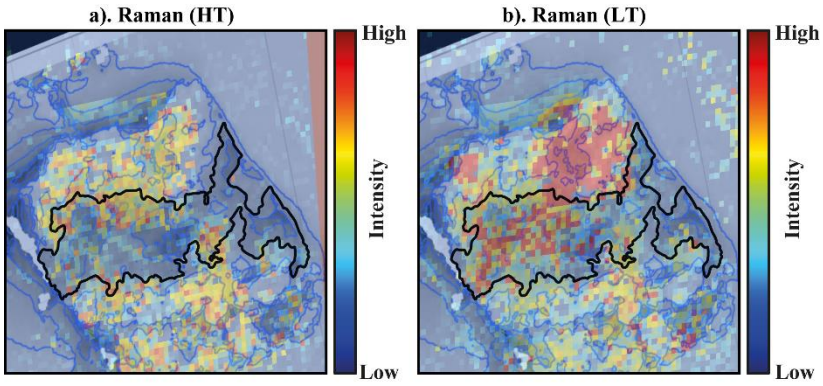

Figure S-8 Raman maps for **(a)** high and **(b)** low topography overlain upon a topographic image of the Murchison sample analysed here. The black line surrounds the boundary between the main areas of high (top 40 µm of sample) and low topography (below top 40 µm) for the sample.

Supplementary Information References

Bokhart, M.T., Nazari, M., Garrard, K.P., Muddiman, D.C. (2018) MSiReader v1. 0: evolving open-source mass spectrometry imaging software for targeted and untargeted analyses. *Journal of the American Society for Mass Spectrometry* 29, 8–16.

Robichaud, G., Garrard, K.P., Barry, J.A., Muddiman, D.C. (2013) MSiReader: an open-source interface to view and analyze high resolving power MS imaging files on Matlab platform. *Journal of the American Society for Mass Spectrometry* 24, 718–721.

Wang, A., Freeman, J.J., Jolliff, B.L. (2015a) Understanding the Raman spectral features of phyllosilicates. *Journal of Raman Spectroscopy* 46, 829–845.

Wang, A., Korotev, R.L., Jolliff, B.L., Ling, Z. (2015b) Raman imaging of extraterrestrial materials. *Planetary and Space Science* 112, 23–34.

Wojdyr, M. (2010) Fityk : a general-purpose peak fitting program. *Journal of Applied Crystallography* 43, 1126–1128.